LEAST-SQUARES REVERSE TIME MIGRATION OF BLENDED DATA WITH LOW-RANK CONSTRAINT ALONG STRUCTURAL DIRECTION

MIN BAI [1], JUAN WU [1], JIANYONG XIE [2] and DONG ZHANG [2]

[1] *School of Resources and Environment, North China University of Water Resources and Electric Power, Zhengzhou 450045, P.R. China. baimin2016@126.com*
[2] *State Key Laboratory of Petroleum Resources and Prospecting, China University of Petroleum, Fuxue Road 18, Beijing 102200, P.R. China. zhangdongconan@163.com*

(Received May 1, 2017; revised version accepted November 8, 2017)

ABSTRACT

Bai, M., Wu, J., Xie, J., and Zhang, D., 2018. Least-squares least reverse time migration of blended data with low-rank constraint along structural direction. *Journal of Seismic Exploration*, 27: 29-48.

The simultaneous-source acquisition has been developed to tremendously improve the marine acquisition efficiency. The economic benefit is compromised by the complexity of recorded seismic data. We propose an effective direct imaging algorithm for migrating the blended simultaneous-source data without preprocessing, i.e., source separation. While the least-squares reverse time migration can help attenuate the crosstalk noise significantly, there are still a huge amount of artifacts existing in the final image. We propose to apply a low-rank constraint to regularize the model during the least-squares inversion. The low-rank constraint is applied along the geological structure of the reflectivity image in order to fully take advantage of the structural patterns of seismic images. Two numerical examples with different complexity validate the effectiveness of the proposed method.

KEY WORDS: simultaneous-source acquisition, least-squares reverse time migration, low-rank constraint, geological structure, crosstalk noise.

INTRODUCTION

The simultaneous-source technique allows simultaneous shooting of marine sources and can obtain a significant acquisition efficiency boost (Abma and Yan, 2009; Chen et al., 2014a). However, this technique will also result in extremely noisy seismic data (Beasley et al., 1998; Mahdad, 2012; Abma, 2014; Chen et al., 2014b; Chen, 2015a; Chen and Fomel, 2015;

0963-0651/18/$5.00

Xue et al., 2017; Zu et al., 2017b,a). One way for solving the strong-noise problem is by first separating the sources and then doing imaging and inversion on the separated sources (Chen, 2015b; Zu et al., 2016; Gan et al., 2016a,b; Qu et al., 2016; Chen et al., 2017a; Chen, 2017). The advantage of this strategy is that the subsequent processing, migration, inversion framework after source separation do not need to be changed since the separated sources are just like the traditionally recorded data. The disadvantage of this method is that numerous effort need to be spent on the source separation process and it is hard to say that there are no damages caused to the useful reflection signals during this step. Another strategy for tackling the interference is by designing robust imaging and inversion algorithms to be applied on simultaneous-source data directly (Verschuur and Berkhout, 2011; Chen et al., 2015b; Gan et al., 2016c; Xue et al., 2016; Chen et al., 2017b).

The least-squares reverse time migration (LSRTM) method has been proven to be one of the most effective methods to migrate the simultaneous-source data (Dai and Schuster, 2011; Xue et al., 2016). The LSRTM algorithm for blended data takes the blending operator into account for formulating the forward operator. Instead of inverting the reflectivity image from the clean traditionally acquired data, it can invert the reflectivity model directly from the blended data. However, due to the serious ill-posedness of the problem and the large interference during two-way wave propagation of the born modeling operator, the inverted image from LSRTM will still contain a lot of artifacts. A regularization method should be used to warrant an acceptable reflectivity model. In this paper, we propose a low-rank constraint to regularize the ill-posed LSRTM for blended data. The low-rank constraint is applied along the geological structure of the image to guarantee the smoothness of the image. We use two numerical examples to demonstrate the performance.

THEORY

Born approximation

Consider the acoustic equation in a constant density media,

$$\left(\frac{1}{v^2}\frac{\partial^2}{\partial t^2} - \nabla^2\right) u = f \quad , \tag{1}$$

where $v(\mathrm{x}, t)$ is the acoustic velocity and $u(\mathrm{x}, t)$ is the wavefield. $f(\mathrm{x}, t)$ is the source function. Considering that v can be expressed as a summation between a smooth background velocity v_0 and a velocity perturbation δv:

$$v = v_0 + \delta v \ , \tag{2}$$

the wavefield can be expressed as a summation between two wavefield components:

$$u = u_0 + \delta u \ , \tag{3}$$

The field u_0 corresponds to the direct wave, while the field δu corresponds to the scattered (or reflected) wave field. Inserting eqs. (2) and (3) into eq. (1):

$$\left(\frac{1}{(v_0 + \delta v)^2} \frac{\partial^2}{\partial t^2} - \nabla^2 \right) (u_0 + \delta u) = f \ , \tag{4}$$

Considering that

$$\frac{1}{(v_0 + \delta v)^2} = \frac{1}{v_0^2} - \frac{2\delta v}{v_0^3} + O(\delta v)^2 \approx \frac{1}{v_0^2} - \frac{2\delta v}{v_0^3}, \tag{5}$$

eq. (4) can be derived as

$$\left[\left(\frac{1}{v_0^2} - \frac{2\delta v}{v_0^3} \right) \frac{\partial^2}{\partial t^2} - \nabla^2 \right] u_0 + \left[\left(\frac{1}{v_0^2} - \frac{2\delta v}{v_0^3} \right) \frac{\partial^2}{\partial t^2} - \nabla^2 \right] \delta u = f. \tag{6}$$

Considering the wave equation with background velocity:

$$\left(\frac{1}{v_0^2} \frac{\partial^2}{\partial t^2} - \nabla^2 \right) u_0 = f \ , \tag{7}$$

eq. (6) can be further simplified as

$$\left(\frac{1}{v_0^2} \frac{\partial^2}{\partial t^2} - \nabla^2 \right) \delta u = \frac{2\delta v}{v_0^3} \frac{\partial^2}{\partial t^2} u_0, \tag{8}$$

by assuming $(2\delta v/{v_0}^3)(\partial^2/\partial t^2)\ \delta v \approx 0$. Comparing eqs. (4) and (8), we see that the reflected field δu generated by a velocity perturbation δc can be interpreted as a secondary wavefield propagating in the unperturbed medium and due to secondary sources excited by the primary field. Let $r = 2\delta v/v_0$, the

linearized wave equation with respect to the reflectivity model can be expressed as

$$\frac{r}{v_0^2}\frac{\partial^2}{\partial t^2}u_0 = \left(\frac{1}{v_0^2}\frac{\partial^2}{\partial t^2} - \nabla^2\right)\delta u. \quad . \tag{9}$$

The regularized inverse problem

In a matrix-vector form, the forward modeling of reflection seismic data using the Born approximation mentioned above can be simply expressed as

$$\mathbf{Lr} = \mathbf{d} \quad , \tag{10}$$

where **d** is the traditionally recorded data, **r** denotes the reflectivity model, and **L** denotes the Born modeling operator.

Simultaneous-source acquisition allows multiple sources to be shot nearly simultaneously to obtain a huge improvement of efficiency. Because of the simultaneous shooting, the traditional data are blended together and the obtained data can be very noisy because of the interferences of neighbor crews. The blending process can be formulated as follows:

$$\mathbf{b} = \Gamma\,\mathbf{d} \quad , \tag{11}$$

where Γ is the blending operator (Mahdad, 2012), which blends different shot records onto one receiver record (node) according to the shot schedules of different shots. **b** denotes the blended data. Combining eqs. (10) and (11), we obtain the classic form of inverse problem:

$$\mathbf{Fr} = \mathbf{b} \quad , \tag{12}$$

where $\mathbf{F} = \Gamma\mathbf{L}$ is the forward operator, **r** is the model to be estimated, and **b** is the observed blended data.

Direct inversion of eq. (12) is not possible because of the extremely large forward matrix and the serious ill-posedness of the inverse problem (Gan et al., 2015; Chen et al., 2015a; Zhong et al., 2016; Liu et al., 2016b,a; Kong et al., 2016). In order to stabilize the inversion, regularization needs to be added to the objective function of least-squares data misfit:

$$J = \| \mathbf{b} - \mathbf{Fr} \|_2^2 + \mu \mathbf{R}(\mathbf{r}) \quad , \tag{13}$$

where $\| \cdot \|_2$ denotes the L_2 norm of an input vector, and **R** denotes a regularization operator applied on **r**. μ denotes a balancing parameter compromising the weights between data misfit and extra regularization. In this paper, we propose a novel structural low-rank constraint for regularizing the reflectivity model. The new constraint is applied so that the seismic image is locally low-rank when mapped to a predefined matrix form that should have a low-rank structure for true reflectivity model. In the shaping regularization framework (Chen et al., 2014a; Xue et al., 2016; Chen and Jin, 2015; Wu et al., 2016), the objective function (13) can be minimized by the following iterative framework.

$$\mathbf{r}_{n+1} = \mathcal{S}(\mathbf{r}_n + \alpha_n \mathbf{s}_n) \quad , \tag{14}$$

where *S* denotes a constraining rank-reduction operator, α_n denotes the step size of model update, and $\mathbf{s}_n$ denotes the updating direction. α_n and $\mathbf{s}_n$ can be obtained from the conjugate-gradient (CG) method. In the next section, we will introduce in detail the constraining operator ***S***.

It is worth mentioning that in eq. (13), **R** is an abstract operator, which we cannot formulate into a matrix form. The constraint **R** is used to enforce the model to be "smooth" along the structural direction. Eq. (13) is a normal regularization form for least-squares inversion. Usually **R** is chosen as $\| \mathbf{r} \|_2$ or $\| \mathbf{Lr} \|_2$ which indicates the traditional Tikhonov regularization. Eq. (13) is convenient only if we can formulate the **R** into a matrix form or an explicit formula. However, for many other cases where the constrain is simple but is not able to be explicitly formulated, it is not easy to use eq. (13) to solve the problem. Shaping regularization framework was proposed by Fomel (2007) for resolving such inconvenience.

Lowrank and structural low-rank decomposition operator

A seismic image can be expressed as a matrix, where m denotes the number of vertical samples and n denotes the number of spatial traces. Suppose the image matrix is composed of useful signal component **S** and artifacts **N**. **S** and **N** are of the same size as **D**. If we assume the artifact (noise) component **N** is composed of small random perturbations, an optimal estimation of **S** following the low-rank approximation theory can be understood as solving the following optimization problem:

$$\min \| \mathbf{N} \|_F^2 \quad ,$$

$$\text{s.t. } \text{rank}(\mathbf{S}) = k \ , \quad \mathbf{D} = \mathbf{S} + \mathbf{N} \ , \tag{15}$$

where k denotes the rank of the signal component. $\|\cdot\|_F$ denotes the Frobenius norm of an input matrix. The problem can be efficiently solved via singular value decomposition (SVD). The observed image matrix **D** can be decomposed into a group of eigen-images via the SVD. The low-rank component **S** can be described with a few eigen-images that are associated with the largest singular values. The noise item **N**, however, will have energy spread over all the eigen-images. This approach is called the low-rank approximation method.

The SVD of the image matrix **D** can be expressed as:

$$\mathbf{D} = \mathbf{U}\mathbf{\Sigma}\mathbf{V}^T \ , \tag{16}$$

Here, **U** is composed of the eigenvectors of $\mathbf{DD}^T$. **V** is composed of the eigenvectors of $\mathbf{D}^T\mathbf{D}$. $\mathbf{\Sigma}$ is a diagonal matrix composed of the decreasing singular values. Let us denote **U**, $\mathbf{\Sigma}$, and **V** in the following form:

$$\begin{aligned} \mathbf{U} &= [\mathbf{u}_1, \mathbf{u}_2, \cdots, \mathbf{u}_n], \\ \mathbf{\Sigma} &= diag(\sigma_1, \sigma_, \cdots, \sigma_n), \\ \mathbf{V} &= [\mathbf{v}_1, \mathbf{v}_2, \cdots, \mathbf{v}_n]. \end{aligned} \tag{17}$$

The vectors $\mathbf{u}_i$ and $\mathbf{v}_i$ are also called the propagation vectors and the eigen-wavelets, respectively. The singular values σ_i are sorted such that $\sigma_1 \geq \sigma_2 \geq \cdots \geq \sigma_n$. They can be obtained by calculating the positive square roots of the eigenvalues of the data covariance matrix $\mathbf{DD}^T$. Eq. (16) can be expressed as:

$$\mathbf{D} = \sum_{i=1}^{n} \lambda_i \mathbf{u}_i \mathbf{v}_i^T \ , \tag{18}$$

where $\mathbf{u}_i\mathbf{v}_i^T$ is the rank-one matrix called the i-th eigenimage of **D**. Thus, from eq. (18), the seismic image can be decomposed into *n* eigenimages, the energy of which corresponds to the value of each element in matrix $\mathbf{\Sigma}$.

We can remove the eliminating the artifacts in seismic images by selecting the first k eigenimages (Freire and Ulrych, 1988; Huang et al., 2016, 2017b,a):

$$\hat{D}_{svd} = \sum_{i=1}^{k} \sigma_i \mathbf{u}_i \mathbf{v}_i^T \ . \tag{19}$$

If a 2D seismic image contains curved events, the image matrix **D** is not low-rank. We need to apply a data mapping in order to create a matrix that have a low-rank property (Chen, 2016). Fig. 1 shows an example where the curved noisy data does not have a low-rank feature, i.e., the singular value matrix does not have distinct large singular values. Fig. 1(a) shows the data. Fig. 1(b) shows the singular values in an amplitude decreasing manner. We can apply a local flattening operator to the data in order to map locally curved events into flattened events. We can create many local windows centered by each trace and flatten the traces in each local window, where it is assumed to have a low-rank feature.

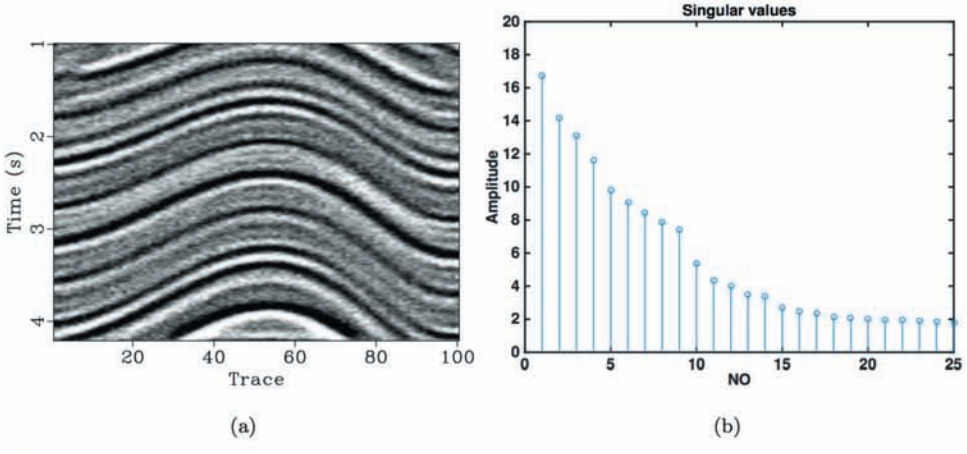

Fig. 1. (a) Noisy data. (b) Singular values corresponding to (a).

We extract one flattened window and show it in Fig. 2a. Fig. 2b shows the corresponding singular values of the flattened gather. It can be seen that this flattened gather has a distinctly large singular value, thus the rank of the data is decided to be 1. By applying the low-rank decomposition eq. (19), we can remove the artifacts (noise), as shown in Fig. 2c. The middle trace in each local window after low-rank approximation is then extracted to output the denoised trace where the local window is centered. We do the data mapping by a recursively predicting strategy. We recall that the target of the data mapping is to create a flattened gather in each local window centered at each trace. Let the width of the window to be 2N + 1, then the central trace d_i can be predicted from its neighbor trace d_{i+j} in a recursive manner following the prediction relation from the p-th to the (p+1)-th trace:

$$u_{p+1}^{v+1} = \left(1 - \frac{\sigma_p \Delta x}{\Delta t}\right) u_p^{v+1} + \frac{\sigma_p \Delta x}{\Delta t} u_p^v, \tag{20}$$

which is derived from the discretized formula of the plane-wave approximation of the wave equation

$$\frac{\partial u}{\partial x} + \sigma \frac{\partial u}{\partial t} = 0 \quad , \tag{21}$$

where *u(t,x)* is the seismic record and σ is local slope. The local slope σ is the a prior knowledge of the morphology of the seismic data, which can be calculated robustly using the plane-wave destruction (PWD) algorithm (Fomel, 2002).

The number of eigenvectors is chosen as one or two at most in the proposed method. As we can see from Fig. 2, after local flattening, the number of distinct singular values is one. So we normally choose one as the rank. All the results shown in the paper come from this rank selection criterion.

The 3D generalization of the proposed method is straightforward. In addition to the 3D generalization of the LSRTM algorithm, the structural operator also requires a 3D extension. In 3D case, the we need to locally flatten the image along the inline and crossline direction by calculating the 3D slope field.

EXAMPLES

We apply the constrained LSRTM framework [eq. (14)] with the structural low-rank approximation operator [eq. (19)] to two numerical examples and demonstrate their corresponding performance.

The first example is shown in Fig. 3. It is a relatively simple example, with curved sendimentary layers and a salt dome in the middle of the model. The recorded data with two simultaneous sources are shown in Fig. 4. Note that the direct ways have been muted for this example by subtracting the raw data by the finite-difference modelled data from homogeneous water velocity.

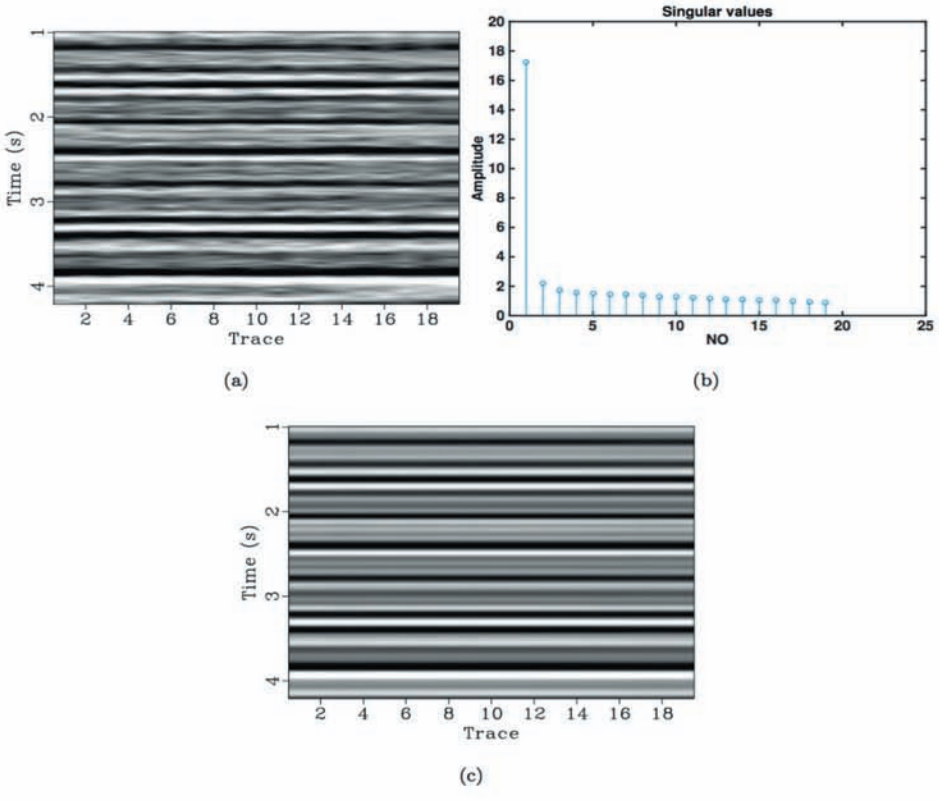

Fig. 2. (a) Data window along the structural direction. (b) Singular values corresponding to (a). (c) Rank-1 approximation result.

The migrated images using LSRTM method and the proposed regularized LSRTM method are shown in Figs. 5a and 5b, respectively. The interferences in the blended data are so strong that the energy between signal and noise are almost equal. The migrated image of LSRTM method still contains a huge amount of artifacts, especially in the shallow part. The migrated image using the proposed method, however, are almost perfect, without any residual artifacts. The local slope used in the structural low-rank constrained LSRTM is obtained from the RTM image. The RTM image of this example is shown in Fig. 6a. The estimated local slope map is shown in Fig. 6b. It is obvious that the RTM image is much noisier than the two inverted images without and with constraint that are shown in Fig. 5. The estimated local slope follows the structure pattern well and is deemed to be accurate enough.

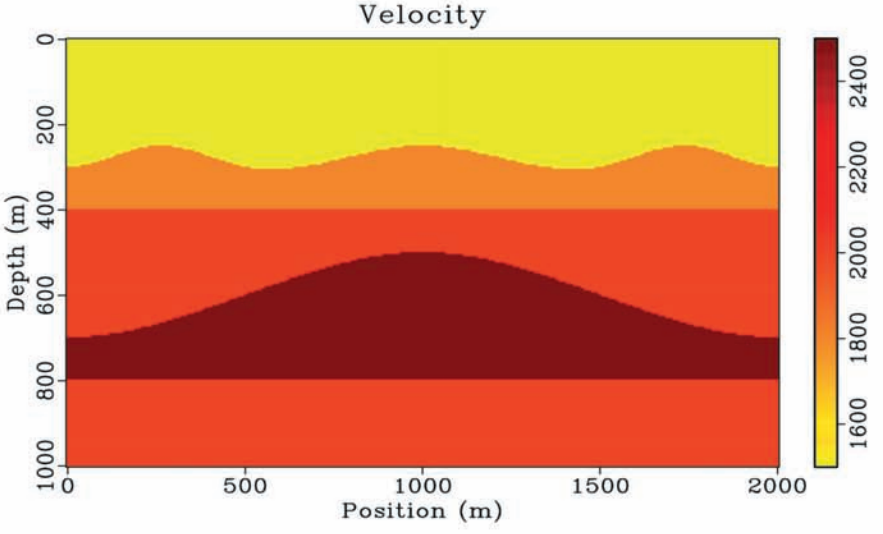

Fig. 3. Velocity model.

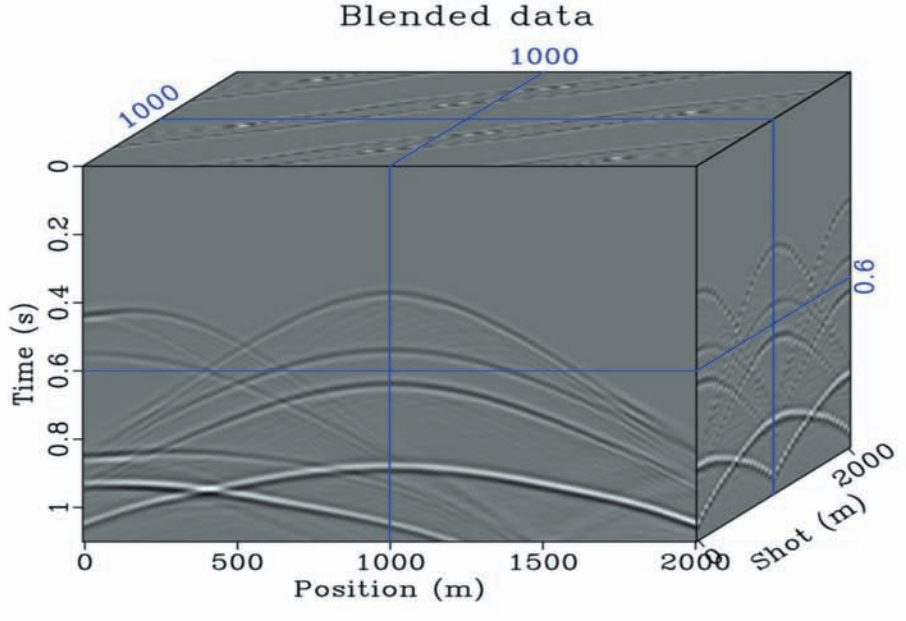

Fig. 4. Recorded blended data.

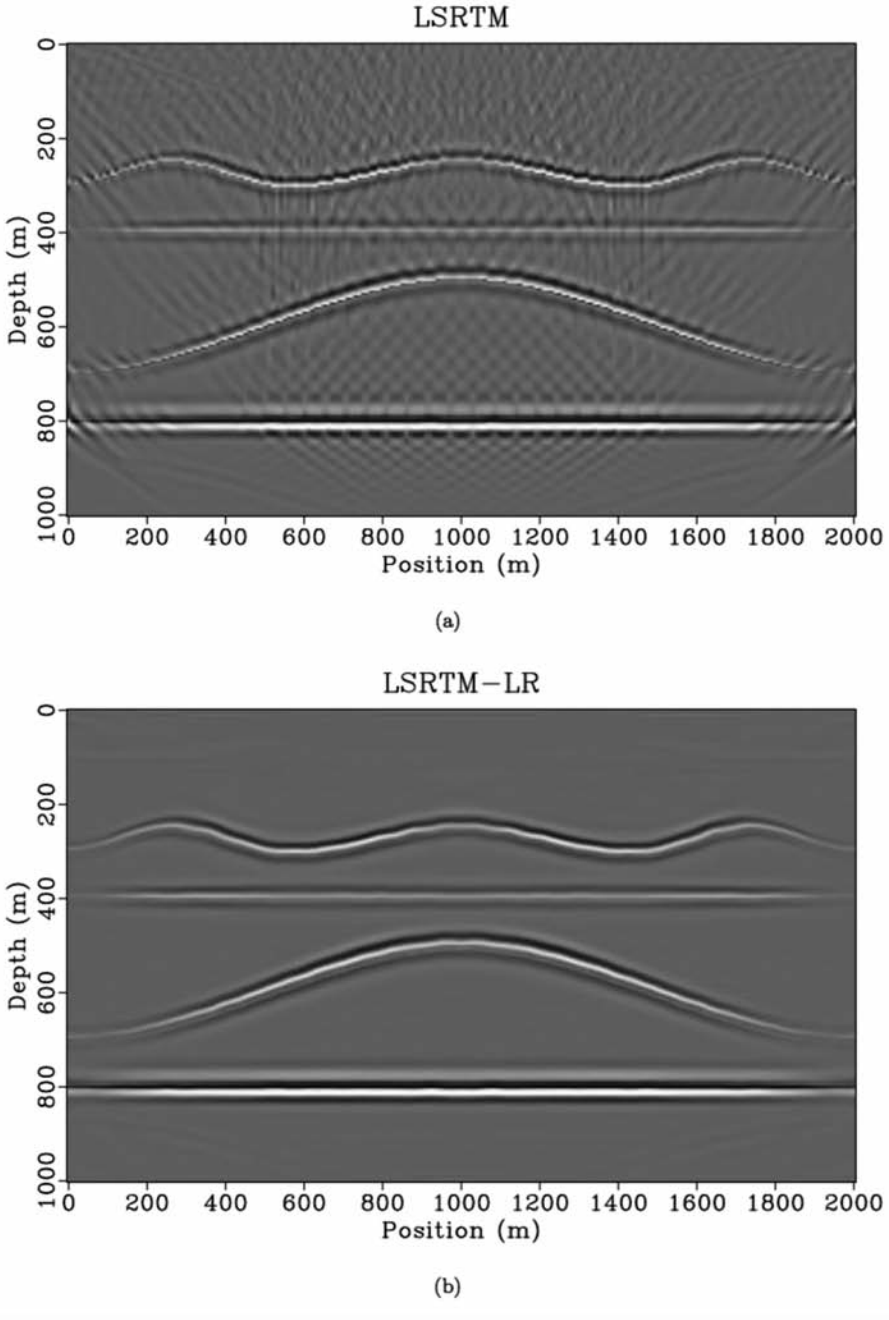

Fig. 5. (a) LSRTM result. (b) LSRTM with lowrank constraint.

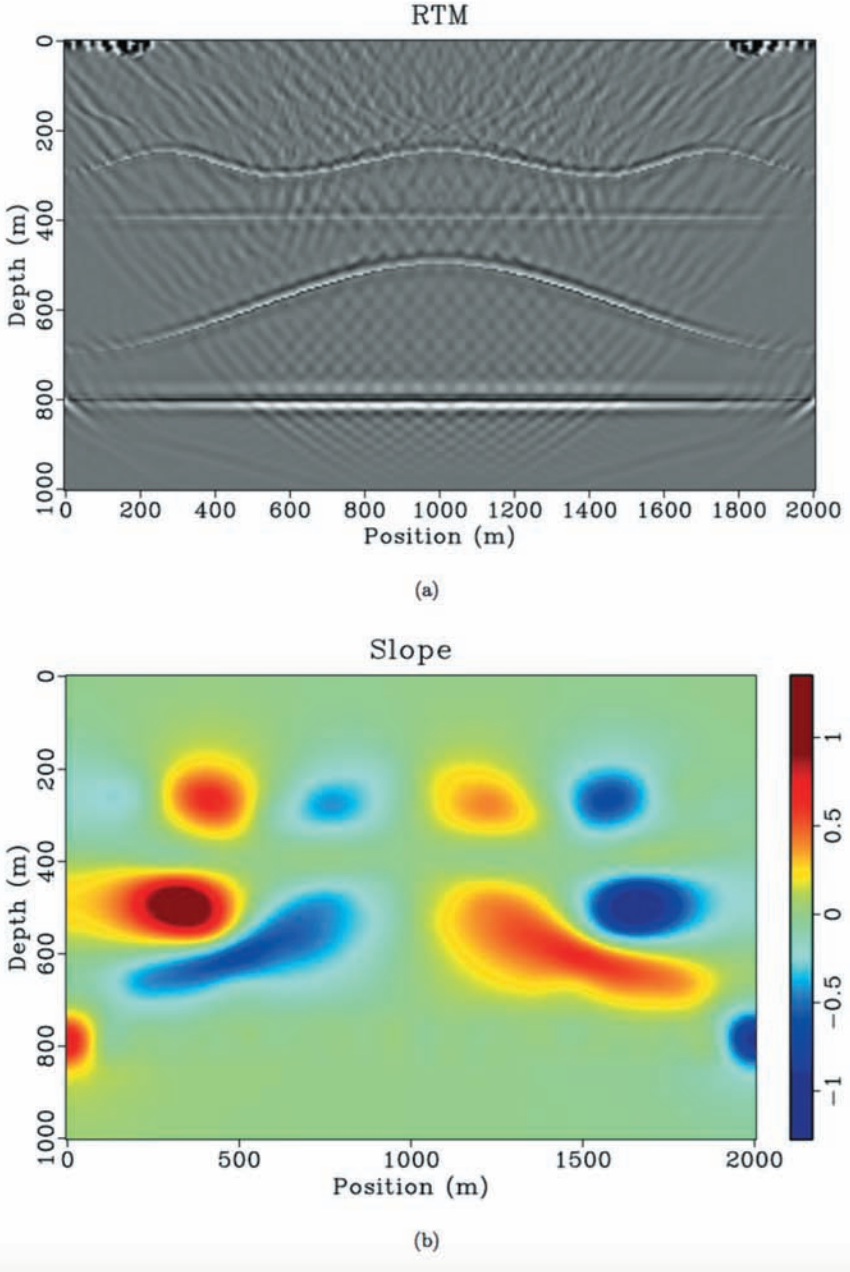

Fig. 6. (a) RTM image. (b) Local slope map that is required by the structural low-rank constraint. (b) is estimated from (a).

The second example is shown in Fig. 7. It is a relatively complex example, with different types of geological features, e.g., pinch-out, curved layers, and potential oil traps. Fig. 8 shows the exact reflectivity model. It is the target we want to obtain in this example. The recorded blended data is shown in Fig. 9. The migrated images using LSRTM and the proposed methods are shown in Figs. 10a and 10b. The migrated image of the low-rank constrained LSRTM obtains a surprisingly successful performance. Fig. 11 shows the slope estimated iteratively in this example. As a comparison, we also show the RTM image in Fig. 12a, where significant migration artifacts caused by the crosstalk noise are existing. Comparing Figs. 10a and 12a, we also conclude that the LSRTM can help suppress the artifacts to some extent and obtain some amplitude balance between shallow and deep reflectors. Fig. 12b shows the RTM image after applying the proposed structural rank-reduction filtering operator. It is salient that the filtering suppress some artifacts but still not adequate to provide a artifacts free image, which explains why we need to apply the shaping filtering during the least-squares inversion. Figs. 13 show a comparison between zoomed images of reflectivity model, RTM image, LSRTM image and image using the proposed method. The comparison further demonstrates the effectiveness of the proposed method.

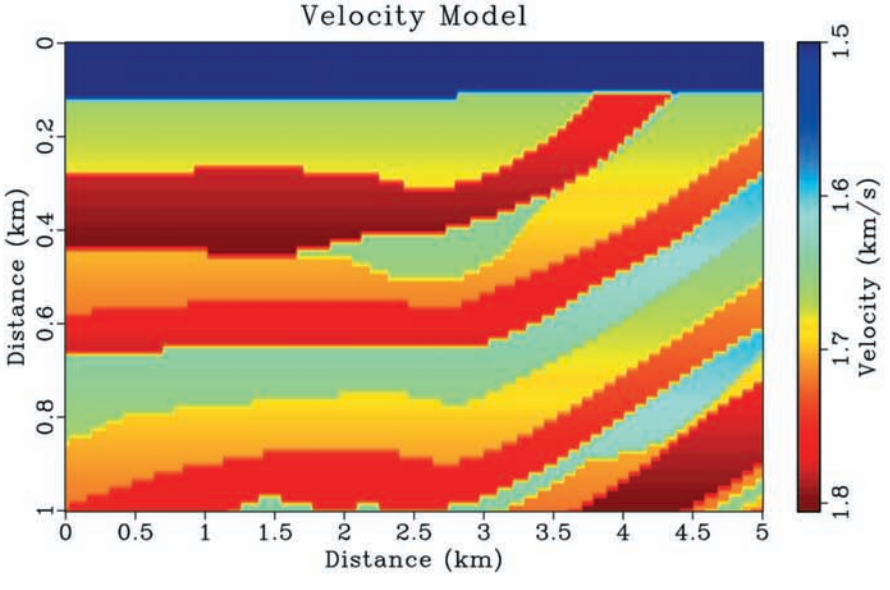

Fig. 7, Complex velocity model.

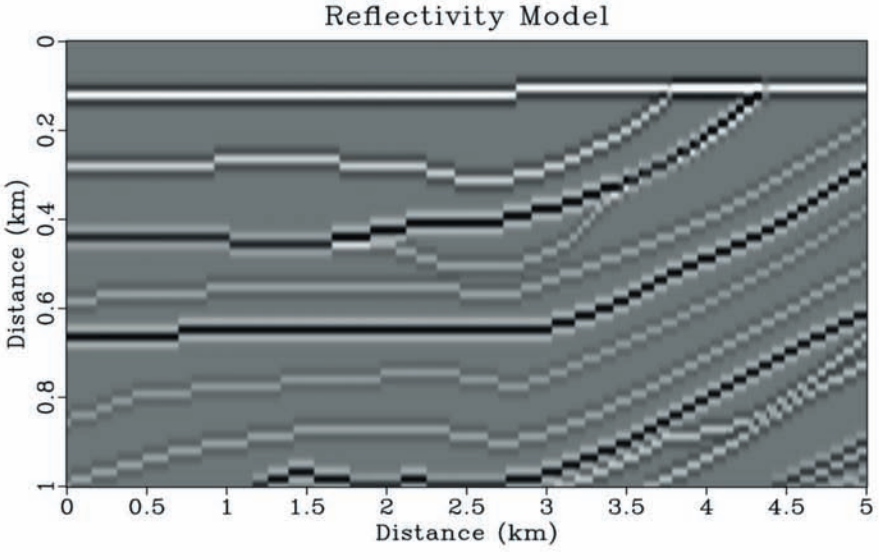

Fig. 8. Exact reflectivity model.

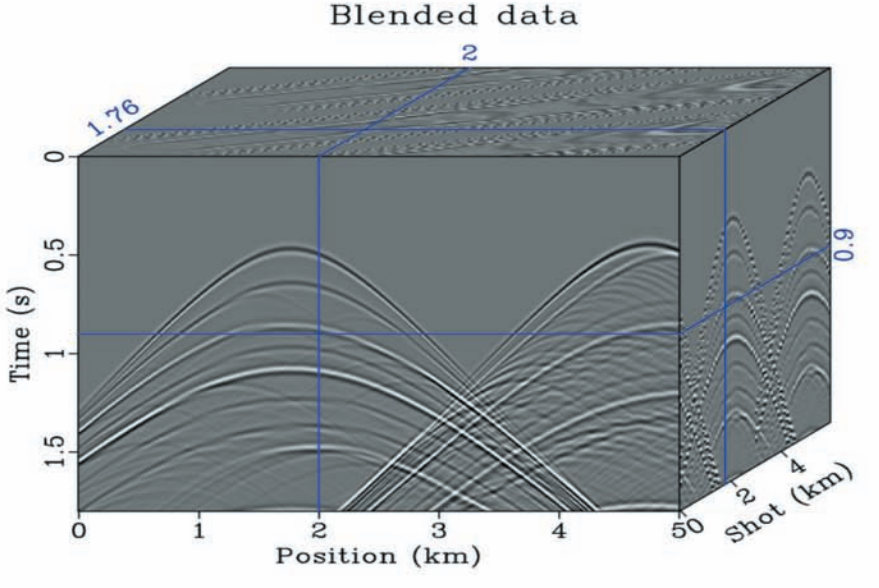

Fig. 9. Recorded blended data from the complex velocity model.

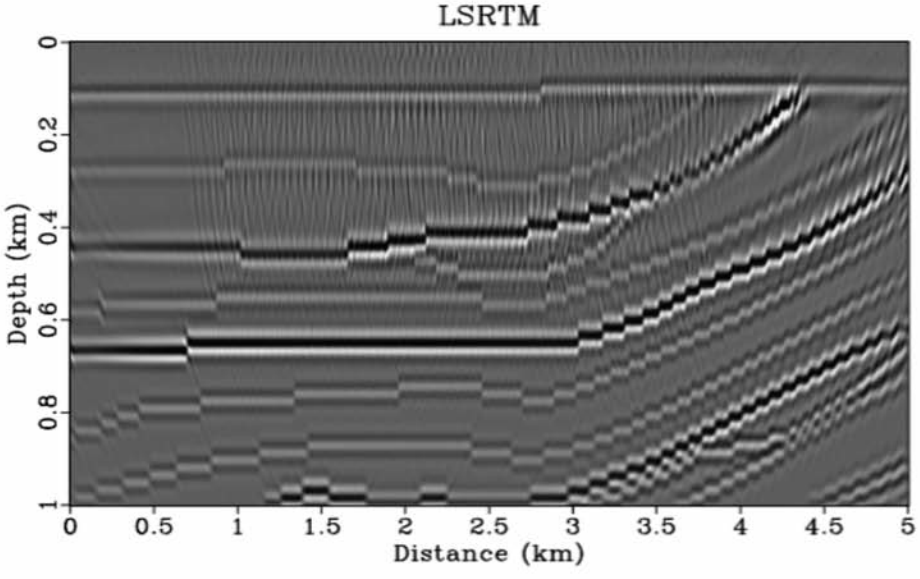

(a)

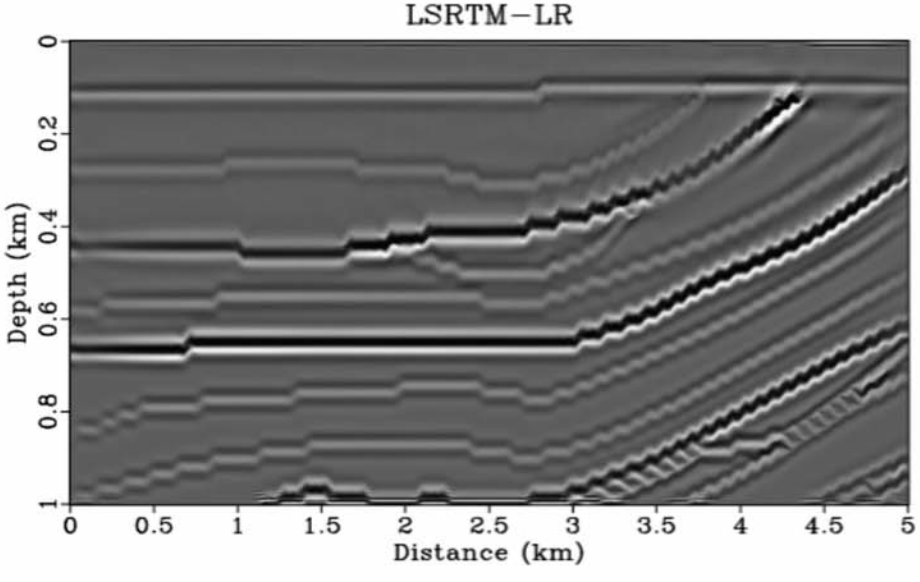

(b)

Fig. 10. (a) LSRTM result. (b) LSRTM with lowrank constraint.

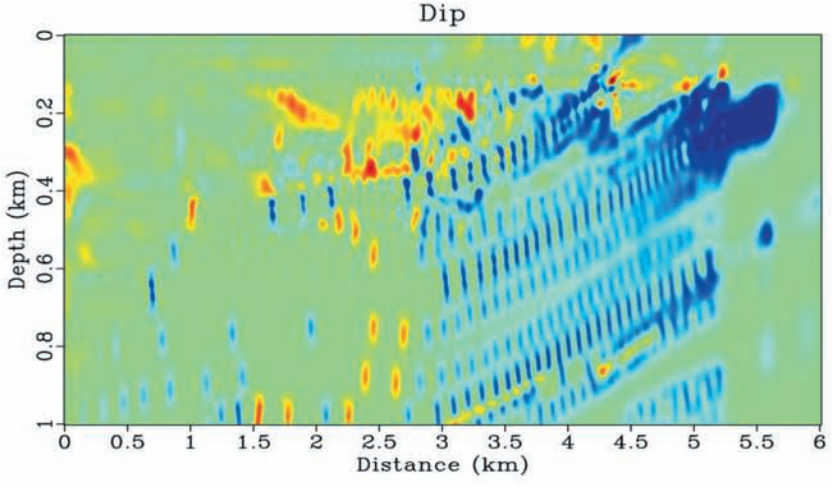

Fig. 11. Estimated dip field.

We use 5 iterations for both examples. Convergence problem is a serious problem we need to face in LSRTM of simultaneous source data. The method can improve the convergence to some extent, but to be honest, it still requires a large number of iterations to converge. In order to compromise the performance and efficiency, we choose 5 iterations (or 10 iterations) for LSRTM. According to our experience, 5-10 iterations is enough to obtain an amplitude-balanced and artifacts-reduced image in the conventional LSRTM method. More iterations can help obtain a more accurate result but the superior performance is not obviously reflected from the image.

CONCLUSION

The simultaneous-source acquisition can reduce the acquisition cost dramatically but at the expense of introducing a significant amount of crosstalk noise in the recorded data. The LSRTM formulates the inverse problem that takes into account the blending operator for solving the reflectivity model directly from recorded blended data. However, there are still a lot of artifacts in the LSRTM image. We have introduced an effective method to regularize the model during inversion via a structural low-rank constraint. The low-rank constraint is applied along geological structure of the image and guarantee the smoothness of the reflectivity model. The numerical examples show that the proposed method is superior to the traditional LSRTM method in obtaining artifacts-free seismic images.

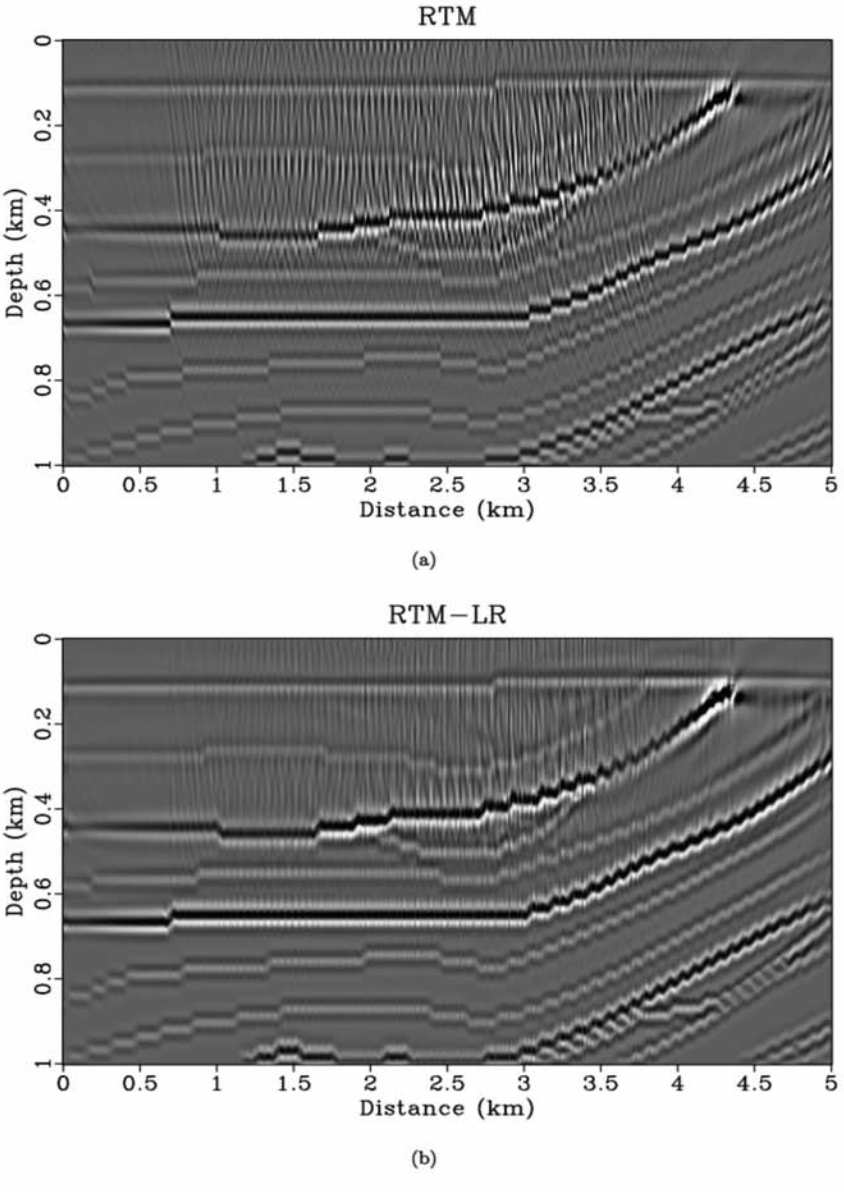

Fig. 12. (a) RTM result. (b) RTM with lowrank filtering.

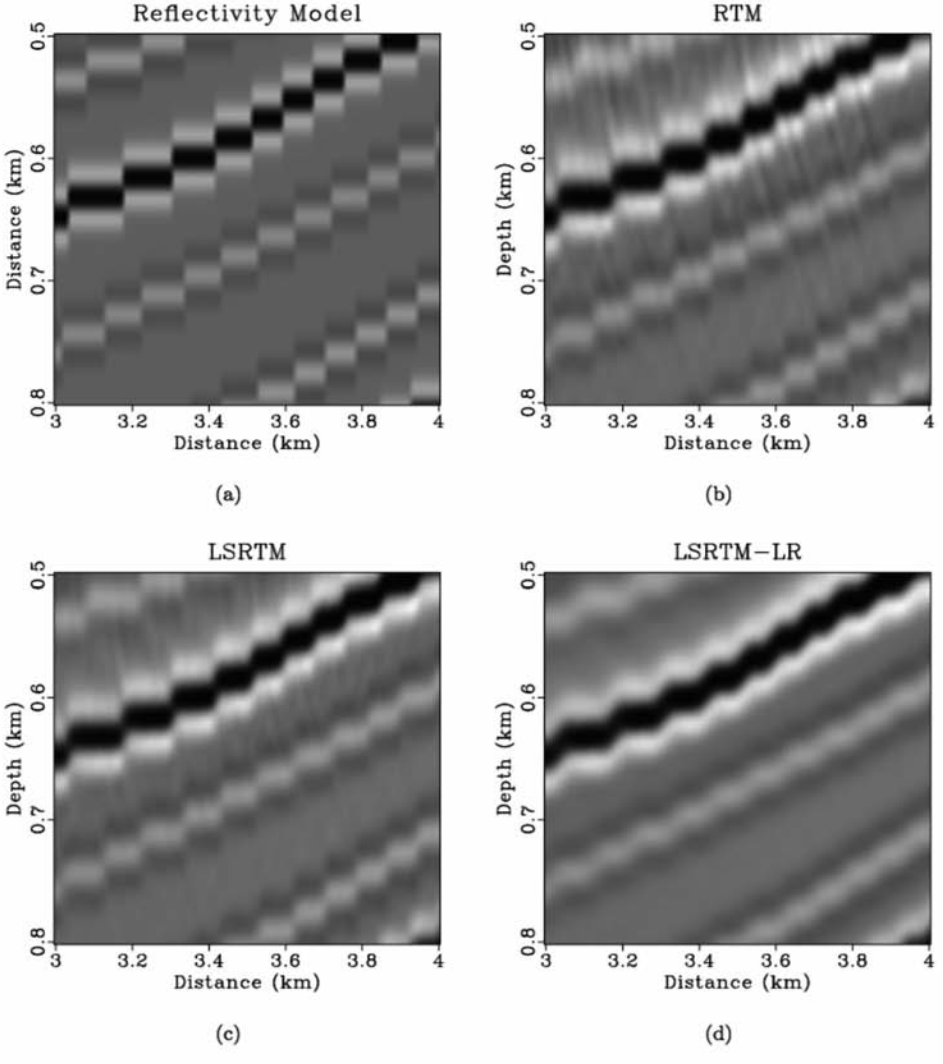

Fig. 13. Zoomed comparison. (a) Exact reflectivity model. (b) RTM image. (c) LSRTM image. (d) LSRTM-LR image.

ACKNOWLEDGEMENTS

The project is supported by the National Natural Science Foundation of China (Grant No. 41704121) and the starting fund at North China University of Water Resources and Electric Power. We would like to thank the helpful and insightful discussions with Yangkang Chen.

REFERENCES

Abma, R., 2014. Shot scheduling in simultaneous shooting. 84th Ann. Internat. SEG Mtg., Denver: 94-98.

Abma, R.L. and Yan, J., 2009. Separating simultaneous sources by inversion. Extended Abstr., 71st EAGE Conf., Amsterdam.

Beasley, C.J., Chambers, R.E. and Jiang, Z., 1998, A new look at simultaneous sources. Expanded Abstr., 68th Ann. Internat. SEG Mtg., New Orleans: 133-135.

Chen, W., Yuan, J., Chen, Y. and Gan, S., 2017a. Preparing the initial model for iterative deblending by median filtering. J. Seismic Explor., 26: 25-47.

Chen, Y., 2015a. Deblending using a space-varying median filter. Explor. Geophys., 46: 332-341.

Chen, Y., 2015b. Iterative deblending with multiple constraints based on shaping regularization. IEEE Geosci. Remote Sens. Lett., 12: 2247-2251.

Chen, Y., 2016. Dip-separated structural filtering using seislet thresholding and adaptive empirical mode decomposition based dip filter. Geophys. J. Internat., 206: 457-469.

Chen, Y., 2017. Fast dictionary learning for noise attenuation of multidimensional seismic data. Geophys. J. Internat., 209: 21-31.

Chen, Y., Chen, H., Xiang, K. and Chen, X., 2017b. Preserving the discontinuities in least-squares reverse time migration of simultaneous-source data. Geophysics, 82(3): S185-S196.

Chen, Y. and Fomel, S., 2015. Random noise attenuation using local signal-and-noise orthogonalization. Geophysics, 80: WD1-WD9.

Chen, Y., Fomel, S. and Hu, J., 2014a. Iterative deblending of simultaneous-source seismic data using seislet-domain shaping regularization. Geophysics, 79: V179-V189.

Chen, Y., Gan, S., Qu, S. and Zu, S., 2015a. Sparse inversion for water bubble removal and spectral enhancement. J. Appl. Geophys., 117: 81-90.

Chen, Y. and Jin, Z., 2015. Simultaneously removing noise and increasing resolution of seismic data using waveform shaping. IEEE Geosci. Remote Sens. Lett., 13: 102-104.

Chen, Y., Yuan, J., Jin, Z., Chen, K. and Zhang, L., 2014b. Deblending using normal moveout and median filtering in common-midpoint gathers. J. Geophys. Engineer., 11: 045012.

Chen, Y., Yuan, J., Zu, S., Qu, S. and Gan, S., 2015b. Seismic imaging of simultaneous-source data using constrained least-squares reverse time migration. J. Appl. Geophys., 114: 32–35.

Dai, W. and Schuster, G.T., 2011. Least-squares migration of multisource data with a deblurring filter. Geophysics, 76: R135–R146.

Fomel, S., 2002. Application of plane-wave destruction filters. Geophysics, 67: 1946-1960.

Fomel, S., 2007. Shaping regularization in geophysical estimation problems. Geophysics, 72: R29-R36.

Freire, S.L.M. and Ulrych, T.J., 1988. Application of singular value decomposition to vertical seismic profiling. Geophysics, 53: 778-785.

Gan, S., Wang, S., Chen, Y. and Chen, X., 2016a. Simultaneous-source separation using iterative seislet-frame thresholding. IEEE Geosci. Remote Sens. Lett., 13, 197-201.

Gan, S., Wang, S., Chen, Y., Chen, X. and Xiang, K., 2016b. Separation of simultaneous sources using a structural-oriented median filter in the flattened dimension. Comput. Geosci., 86: 46-54.

Gan, S., Wang, S., Chen, Y., Qu, S. and Zu, S., 2016c. Velocity analysis of simultaneous-source data using high-resolution semblance-coping with the strong noise. Geophys. J. Internat., 204: 768-779.

Gan, S., Wang, S., Chen, Y., Zhang, Y. and Jin, Z., 2015. Dealiased seismic data interpolation using seislet transform with low-frequency constraint. IEEE Geosci. Remote Sens. Lett., 12: 2150-2154.

Huang, W., Wang, R., Chen, X. and Chen, Y., 2017a. Double least squares projections method for signal estimation. IEEE Transact. Geosci. Remote Sens., 55: 4111-4129.

Huang, W., Wang, R., Chen, Y., Li, H. and Gan, S., 2016. Damped multichannel singular spectrum analysis for 3D random noise attenuation. Geophysics, 81(4): V261-V270.

Huang, W., Wang, R., Yuan, Y., Gan, S. and Chen, Y., 2017b. Signal extraction using randomized-order multichannel singular spectrum analysis: Geophysics, 82, no. 2, V59-V74.

Kong, D., Peng, Z., He, Y. and Fan, H., 2016. Seismic random noise attenuation using directional total variation in the shearlet domain. J. Seismic Explor., , 25: 321-338.

Liu, C., Wang, D., Hu, B., and Wang, T., 2016a. Seismic deconvolution with shearlet sparsity constrained inversion. J. Seismic Explor., 25: 433-445.

Liu, W., Cao, S., Gan, S., Chen, Y., Zu, S. and Jin, Z., 2016b. One-step slope estimation for dealiased seismic data reconstruction via iterative seislet thresholding. IEEE Geosci. Remote Sens. Lett., 13: 1462-1466.

Mahdad, A., 2012. Deblending of Seismic Data. Ph.D. thesis, TU Delft.

Qu, S., Zhou, H., Liu, R., Chen, Y., Zu, S., Yu, S., Yuan, J. and Yang, Y., 2016. Deblending of simultaneous-source seismic data using fast iterative shrinkage-thresholding algorithm with firm-thresholding. Acta Geophys., 64: 1064-1092.

Verschuur, D.J. and Berkhout, A.J., 2011. Seismic migration of blended shot records with surface-related multiple scattering. Geophysics, 76: A7-A13.

Wu, J., Wang, R., Chen, Y., Zhang, Y., Gan, S. and Zhou, C., 2016. Multiples attenuation using shaping regularization with seislet domain sparsity constraint. J. Seismic Explor., 25: 1-9.

Xue, Y., Man, M., Zu, S., Chang, F. and Chen, Y., 2017. Amplitude-preserving iterative deblending of simultaneous source seismic data using high-order radon transform. J. Appl. Geophys., 139: 79-90.

Xue, Z., Chen, Y., Fomel, S. and Sun, J., 2016. Seismic imaging of incomplete data and simultaneous-source data using least-squares reverse time migration with shaping regularization. Geophysics, 81: S11-S20.

Zhong, W., Chen, Y., Gan, S. and Yuan, J., 2016. L1/2 norm regularization for 3D seismic data interpolation. J. Seismic Explor.: 257-268.

Zu, S., Zhou, H., Chen, H., Zheng, H. and Chen, Y., 2017a. Two field trials for deblending of simultaneous source surveys: why we failed and why we succeeded? J. Appl. Geophys., 143: 182-194.

Zu, S., Zhou, H., Chen, Y., Qu, S., Zou, X., Chen, H. and Liu, R., 2016. A periodically varying code for improving deblending of simultaneous sources in marine acquisition. Geophysics, 81: V213-V225.

Zu, S., Zhou, H., Li, Q., Chen, H., Zhang, Q., Mao, W. and Chen, Y., 2017b. Shot-domain deblending using least-squares inversion. Geophysics, 82(4): V241-V256